NAVAL POSTGRADUATE SCHOOL
Monterey, California

THESIS

QUANTITATIVE EVALUATION OF THE LIMITATIONS OF THE RADIATION BOUNDARY ELEMENTS IN THE FINITE ELEMENT CODE ATILA

by

Panagiotis A. Sinanoglou

June 1996

Thesis Advisor:	Steven R. Baker
Co-Advisor:	Clyde L. Scandrett

Approved for public release; distribution is unlimited.

REPORT DOCUMENTATION PAGE		Form Approved OMB No. 0704-0188

1. AGENCY USE ONLY (Leave Blank)	2. REPORT DATE June 96	3. REPORT TYPE AND DATES COVERED Master's Thesis

4. TITLE AND SUBTITLE
QUANTITATIVE EVALUATION OF THE LIMITATIONS OF THE RADIATION BOUNDARY ELEMENTS IN THE FINITE ELEMENT CODE ATILA

5. FUNDING NUMBERS

6. AUTHOR(S)
Sinanoglou, Panagiotis A.

7. PERFORMING ORGANIZATION NAME(S) AND ADDRESS(ES)
Naval Postgraduate School
Monterey, CA 93943-5000

8. PERFORMING ORGANIZATION REPORT NUMBER

9. SPONSORING/MONITORING AGENCY NAME(S) AND ADDRESS(ES)

10. SPONSORING/MONITORING AGENCY REPORT NUMBER

11. SUPPLEMENTARY NOTES

The views expressed in this thesis are those of the author and do not reflect the official policy or position of the Department of Defense or the U.S. Government

12A. DISTRIBUTION/AVAILABILITY STATEMENT

Approved for public release; distribution is unlimited

12b. DISTRIBUTION CODE

13. ABSTRACT *(maximum 200 words)*

A quantitative evaluation of the limitations of the radiation boundary elements in the finite element code ATILA [Ref. 1] has been performed. Five three-dimensional models were employed, each representing a rigid spherical solid surrounded by water. Monopolar, dipolar and quadrupolar incident spherical waves were introduced and the corresponding scattered waves were computed using the ATILA code and an exact analytical solution.

The dimensionless parameters that characterize the problem are ka, kL, and kR where k is the wavenumber of sound in water, a is the radius of the scatterer, R is the outer fluid mesh radius, and L is the thickness of the fluid layer. The range of values investigated were $kR = 1.5, 2.5, 4.0$, $ka = 0.5, 1.0, 2.0$ and $kL = 0.5, 1.0$.

For axially symmetric incident fields, the maximum normalized errors occurred at the poles and were 9%, 12%, and 6% respectively. Furthermore, the errors for monopolar and dipolar incident fields were strongly influenced by the location of the radiation boundary (kR), less so by the scatterer's radius (ka); specifically the error decreases with increasing kR and/or ka. The errors for quadrupolar incident fields do not exhibit any significant dependence on kR or ka. The errors for all the axially symmetric incident fields were not affected by variations of the element's size (kL). For non-axially symmetric incident fields, the maximum deviation occurred at the equatorial points and was less than 5.5%.

Further investigation using a two-dimensional model is proposed in order to determine the range of values of ka, kL, and kR which will result in negligibly small errors.

14. SUBJECT TERMS
ATILA, finite element code, radiation boundary elements, monopolar, dipolar and quadrupolar incident fields

15. NUMBER OF PAGES
65

16. PRICE CODE

17. SECURITY CLASSIFICATION OF REPORT Unclassified	18. SECURITY CLASSIFICATION OF THIS PAGE Unclassified	19. SECURITY CLASSIFICATION OF ABSTRACT Unclassified	20. LIMITATION OF ABSTRACT UL

QUANTITATIVE EVALUATION OF THE LIMITATIONS OF THE RADIATION BOUNDARY ELEMENTS IN THE FINITE ELEMENT CODE ATILA

Panagiotis A. Sinanoglou
Lieutenant , Hellenic Navy
B.S., Hellenic Naval Academy, 1985

Submitted in partial fulfillment
of the requirements for the degree of

MASTER OF SCIENCE IN APPLIED PHYSICS

from the

NAVAL POSTGRADUATE SCHOOL
June 1996

ABSTRACT

A quantitative evaluation of the limitations of the radiation boundary elements in the finite element code ATILA [Ref. 1] has been performed. Five three-dimensional models were employed, each representing a rigid spherical solid surrounded by water. Monopolar, dipolar and quadrupolar incident spherical waves were introduced and the corresponding scattered waves were computed using the ATILA code and an exact analytical solution.

The dimensionless parameters that characterize the problem are ka, kL, and kR where k is the wavenumber of sound in water, a is the radius of the scatterer, R is the outer fluid mesh radius, and L is the thickness of the fluid layer. The range of values investigated were $kR=1.5, 2.5, 4.0$, $ka=0.5, 1.0, 2.0$ and $kL=0.5, 1.0$.

For axially symmetric incident fields, the maximum normalized errors occurred at the poles and were 9%, 12%, and 6%, respectively. Furthermore, the errors for monopolar and dipolar incident fields were strongly influenced by the location of the radiation boundary (kR), less so by the scatterer's radius (ka); specifically, the error decreases with increasing kR and/or ka. The errors for quadrupolar incident fields do not exhibit any significant dependence on kR or ka. The errors for all the axially symmetric incident fields were not affected by variations of the element's size (kL). For non-axially symmetric incident fields, the maximum deviation occurred at the equatorial points and was less than 5.5%.

Further investigation using a two-dimensional model is proposed in order to determine the range of values of ka, kL, and kR which will result in negligibly small errors.

TABLE OF CONTENTS

ACKNOWLEDGMENTS

I. INTRODUCTION

The investigation described in this thesis is part of an ongoing research project in the numerical modeling of arbitrary densely packed, random volumetric active sonar arrays [Ref. 1]. The technique employed is an extension of the so-called T-matrix method, which has been applied to other scattering problems [Ref. 2]. This method rigorously accounts for multiple scattering to all orders. To apply the T-matrix method to the problem of active sonar array performance prediction, it is necessary to compute the radiating and scattering properties of a single array element in a free field environment. To accomplish this for a real transducer, the ATILA [Ref. 3] finite element code is employed.

ATILA is a French finite element code especially developed for the analysis of underwater acoustic transducers. This code was written by engineers at the Institut Superieur d'Electronique du Nord (ISEN), Lille, France and is in use by U.S. scientists within and outside the Navy working on U.S. Navy-sponsored research.

Computation of the radiating and scattering properties of a sonar transducer using ATILA involves building a finite-element model representing the transducer and surrounding it by a finite-element mesh representing water, which is terminated by so-called "radiation boundary elements". The radiation boundary elements are intended to "absorb" all incident acoustic radiation. In practice, they perform this function less than perfectly. This has a direct effect on the computation of a transducer's radiating and scattering properties.

The present investigation focuses on the evaluation of ATILA's radiation boundary elements. For this purpose, a three dimensional spherical fluid mesh, surrounding a spherical rigid body and terminated by radiation boundary elements is studied. An incident spherical wave consisting of a single component of a multipolar acoustic field strikes the sphere, and the resulting scattered wave field is calculated using ATILA. The amounts of acoustic field in

the intended outgoing component and in other multipolar components are then analyzed. The influence on the results of the fluid mesh element size, fluid mesh inner radius, and fluid mesh outer radius relative to the acoustic wavelength are investigated and quantitative guidelines developed in order to minimize the effect of imperfect absorption.

The remainder of this thesis is divided into four chapters. Chapter II describes the theory involved in the finite element analysis, the possible types of analyses that can be performed, particularly the harmonic analysis of a radiating spherical structure excited by an incident spherical wave.

Chapter III describes the three dimensional spherical models which were employed. Chapter IV presents and discusses the scattering results for different incident multipolar components and the influence of element size and mesh inner and outer radius. Chapter V concludes the thesis. Appendix A contains the C program used to analytically calculate the pressure scattered from the spherical boundary for pressure release and rigid surface boundary conditions. Appendix B presents the FORTRAN code used in ATILA for the generation of the spherical incident pressure wave.

II. THEORY

A.   GENERAL PRESENTATION OF ATILA VERSION 5.03

The finite element method is a technique that provides numerical solutions for boundary value problems and field calculations. [Refs. 4,5,6,7,8] ATILA is a finite element code developed specifically for the analysis of sonar transducers.

The ATILA code is able to perform:

1.   elastic or piezoelectric structures modeling,

2.   magnetostrictive structures modeling,

3.   periodic structures modeling,

following a general formulation shown in Figure 1 (after [Ref. 3]), to model an underwater acoustic transducer.
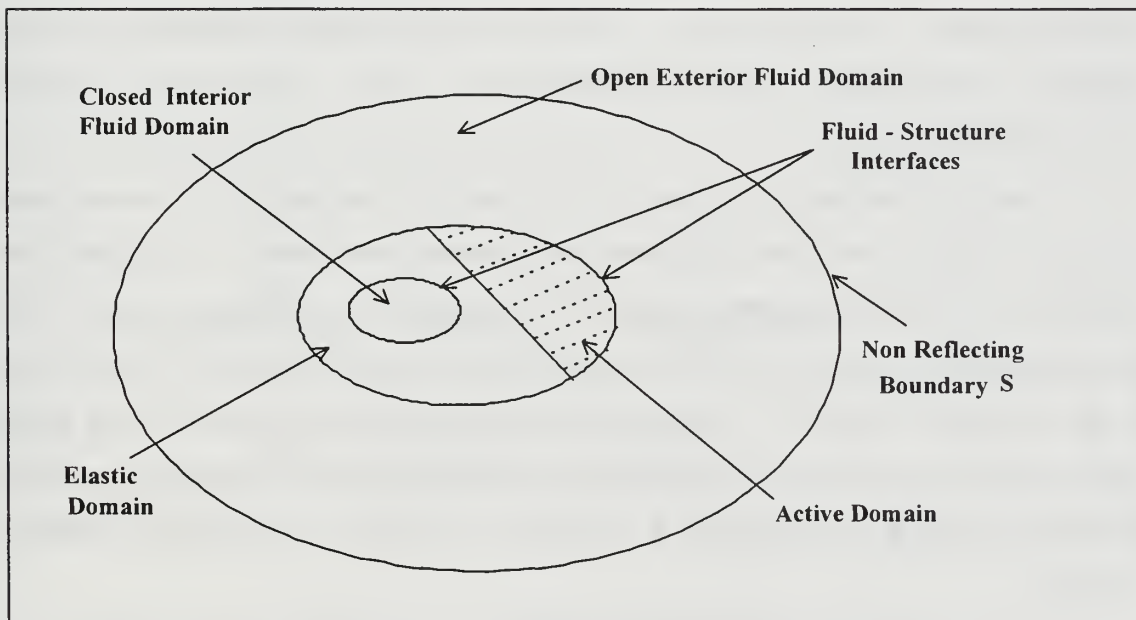
Figure 1. ATILA general formulation. After Ref. [3]

The ATILA code is based on the separation of the physical problem under consideration into a discrete number of elements which are in turn described by their nodes, in a given order. For each node there are a number of degrees of freedom (d.o.f.) that can be specified using certain boundary conditions. The elements, nodes, and the specific node-numbering order, is referred to as the topology of the problem.

An ATILA job organization is carried out in several steps, as follows:

1. Model definition.
2. Mesh generation.
3. Data file preparation.
4. Running a job.
5. Result file postprocessing.

First of all, the type of analysis to be performed has to be specified, for example, harmonic analysis of a solid structure excited by an impinging wave. The type of elements that are required to describe the fluid and structure domain are then chosen. ATILA includes a library of 46 different elements to model composite, piezoelectric, fluid, magnetostrictive, coupling FEM-BEM, interface, and radiation dampers.

The mesh generation procedure includes the assignment of coordinates for each node and the node-numbering order for each element. Throughout this procedure the whole physical problem is discretized into elements which allow the representation and modeling of many different geometrical shapes and lines, as, for example, PRIS15F, a fifteen-node isoparametric triangular base prism used to model homogenous fluid media, or TRIA06R, a six node isoparametric triangular element to prescribe a monopolar, dipolar, or multipolar radiation condition.

One of the facilities of the ATILA code is the MOSAIQUE preprocessor. This routine enables the use of super-elements and generates all the necessary elements and node data for ATILA.

The data file includes all the neccessary input data such as the type of analysis, the material properties, the node coordinates, the elements, the boundary conditions, the loading data, and possibly the plane wave data, to carry out the analysis.

Running an ATILA job involves calling up the subroutines to compute elementary matrices, solve equations and display the results.

The available results file, if desired, can be postprocessed to create graphic displays of the structure, contours of constant value for potentials, pressures, and displacements. A simple flow chart of an ATILA job is shown in Figure 2 (after [Ref. 3]).
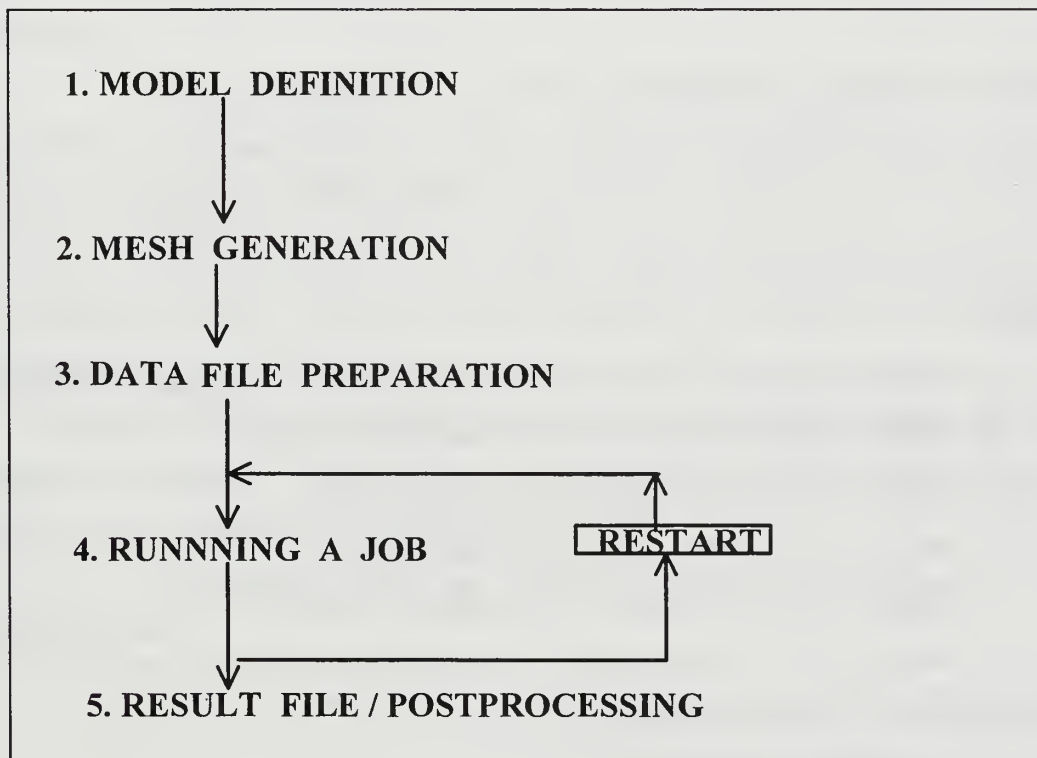
Figure 2. Flow chart of an ATILA job. After Ref.[3]

B. ATILA FINITE ELEMENT COMPUTATION FOR RADIATING AND SCATTERING PROBLEMS

1. General Elastic or Piezoelectric Structures Modeling

A large number of analyses can be performed. These are based upon the complete set of equations of elasticity in the structure, the Helmholtz equation in the fluid, and Poisson's equation in the elastic or piezoelectric material. Appropriate radiation boundary conditions are applied on the surface which surrounds the fluid domain.

The unknown quantities are the nodal values of the displacement field $\underline{U}$ in the whole structure, the electric potential Φ in the piezoelectric material, and the pressure $\underline{P}$ in the fluid. The system of equations is written in matrix form:

$$
\begin{bmatrix}
([K_{uu}] - \omega^2[M]) & [K_{u\phi}] & -[L] \\
[K_{u\phi}]^T & [K_{\phi\phi}] & [0] \\
-\rho^2 c^2 \omega^2 [L]^T & [0]^T & ([H] - \omega^2[M_1])
\end{bmatrix}
\begin{bmatrix}
\underline{U} \\
\underline{\Phi} \\
\underline{P}
\end{bmatrix}
=
\begin{bmatrix}
\underline{F} \\
-\underline{q} \\
\rho c^2 \underline{\psi}
\end{bmatrix}
$$

where:

$\underline{U}$: vector of the nodal values of the components of the displacement field.

$\underline{\Phi}$: vector of the nodal values of the electric potential.

$\underline{P}$: vector of the nodal values of the pressure field.

$\underline{F}$: vector of the nodal values of the applied forces.

$\underline{q}$: vector of the nodal values of the electric charges.

$\underline{\psi}$: vector of the nodal values of the integrated normal derivative of the pressure on the surface boundary S.

$[K_{uu}]$: stiffness matrix.

$[K_{u\phi}]$; piezoelectric matrix.

$[K_{\phi\phi}]$: dielectric matrix.

$[M]$: consistent mass matrix.

$[H]$: fluid (pseudo-)stiffness matrix.

$[M_1]$: consistent (pseudo-)fluid mass matrix.

$[L]$: coupling matrix at the fluid structure interface (connectivity matrix).

$[0]$: zero matrix.

ω: angular frequency.

ρ: fluid density.

c: fluid sound speed.

T: means transposed.

ATILA is able to perform:

1.   Static analysis of an elastic, piezoelectric, or hydroelastic system, where the displacement field and/or the electric potential or the pressure fields are required.

2.   Modal analysis of an elastic, piezoelectric, hydroelastic system, where the eigenfrequencies, the resonance and antiresonance frequencies, and the normal modes are computed.

3.   Harmonic analysis of a driven elastic or piezoelectric structure, or the scattering of an arbitrary incident wave by an elastic or piezoelectric structure.

A scattered wave analysis of a spherical pressure wave incident on a solid structure is required to investigate the performance of the radiation boundary elements, and is presented in the following section.

2.   Harmonic Analysis of a Solid Structure Excited by an Impinging Wave

In this type of analysis, the real and imaginary parts of the pressure field ($\underline{P}$), the displacement field ($\underline{U}$), the potential ($\underline{\Phi}$), and the electric current ($j\omega\underline{Q}$) are computed. The pressure ($\underline{P}$) and the flux $\rho c^2 \underline{\Psi}$, are split into incident and scattered parts. The normal derivative of the incident pressure on the surface boundary S is written $\underline{\Psi}_i = [D]\dfrac{\partial P_i}{\partial n}$, where $[D]$ is a matrix obtained by assembling the damping elements on the surface, provided by the code.

The incident pressure field (P_i) is provided via a FORTRAN function "INCPRE (x,y,z,k)", included at the end of the main program by the user as shown in Appendix B, after [Ref 2]. Utilization of a user-provided incident pressure allows the excitation of the structure with an incident wave of any kind, while the default function provided with ATILA generates a plane wave e^{jkx} traveling from the positive to the negative direction along the Ox axis ($e^{j\omega t}$ time harmonic dependence is assumed).

By assigning a specific entry in the ATILA code, we are able to compute the total pressure or just the scattered one, utilizing the "TOTAL" or "SCATTERED" attribute, respectively.

The equations of elasticity in the structure, the Helmoltz equation in the fluid, and Poisson's equation in the solid material are written in matrix form :

$$
\begin{bmatrix}
([K_{uu}] - \omega^2[M]) & [K_{u\phi}] & -[L] \\
[K_{u\phi}]^T & [K_{\phi\phi}] & [0] \\
-[L]^T & [0]^T & \left(\dfrac{[H]}{\rho^2 c^2 \omega^2} - \dfrac{[M_1]}{\rho^2 c^2} \right)
\end{bmatrix}
\begin{bmatrix}
\underline{U} \\
\underline{\Phi} \\
\underline{P_{es}}
\end{bmatrix}
=
\begin{bmatrix}
\underline{F} - [L]P_i \\
-\underline{Q} \\
\dfrac{1}{\rho^2 c^2 \omega^2}[G]\underline{P_{es}} + \dfrac{[D]}{\rho^2 \omega^2}\dfrac{\partial P_i}{\partial n} + \left(\dfrac{[H]}{\rho^2 c^2 \omega^2} - \dfrac{[M_i]}{\rho^2 c^2} \right)\underline{P_i}
\end{bmatrix}
$$

where:

$\underline{P_{es}}$: vector of the nodal values of the elastic scattered pressure field,

$\underline{P_i}$: vector of the nodal values of the incident pressure field,

[G]: frequency dependent complex linear matrix,

[D]: matrix of the damping elements.

Furthermore, the internal losses of the material used can be taken into account throughout a specified program entry "SKYLINE COMPLEX" and when no losses are required, with "SKYLINE REAL", respectively.

8

III. THREE DIMENSIONAL SPHERICAL MODELS

A.   INTRODUCTION

In order to evaluate ATILA's radiation boundary elements, we first developed a family of three-dimensional spherical models.   These models simulate a spherical rigid structure surrounded by an infinite fluid environment.

A total of five models were employed.   All models are composed of an inner spherical boundary representing a rigid solid, several concentric spherical fluids layers, and an outer spherical boundary composed of radiation boundary elements (dampers), each representing a semi-infinite fluid region.

B.   DESCRIPTION OF MODELS

The models developed are distinguished by their values of the inner radius a, the number and thickness L of each fluid layer, and the outer radius R. The appropriate dimensionless forms for these parameters are ka, kL, kR, where $k = \frac{\omega}{c}$ is the acoustic wavenumber.   Table 1 lists the properties of each model used in the investigation.

Model 1 had already been used in the calculation of the transition matrix for the scattering of acoustic waves from a thin elastic spherical shell [Ref. 2]. This model contains four fluid layers of two different thicknesses.   To separately investigate the influence of each of the dimensionless parameters (ka, kR, kL), four additional models were created.

Model 2 serves as a reference model.   Each of models 3 through 5 is distinguished from model 2 in that the value of only one of ka, kL, kR is changed.

	Model 1 Original	Model 2 Basic	Model 3 ka	Model 4 kL	Model 5 kR
Wavenumber k in meters^{-1}	2	1	1	1	1
Radius a in meters	0.5	0.5	1.0	0.5	0.5
Scatterers Radius ka	1.0	0.5	1.0	0.5	0.5
Number of Fluid Layers	2 of L = 0.25 2 of L = 0.5	4 of L = 0.5	3 of L = 0.5	2 of L= 1.0	2 of L = 0.5
Element's Size kL	1.0	0.5	0.5	1.0	0.5
Radiation Boundary kR	4.0	2.5	2.5	2.5	1.5

Table 1. Properties of each model used in the investigation.

The solid structure is modeled by specifying a zero-flux or boundary condition on the scatterer surface (interface between solid and fluid domain). This is the default condition.

For radiation problems, the fluid mesh outer limit must be spherical. Therefore, the surrounding solid structure fluid is modeled with a spherical surface of dimensionless radius kR = 2.5 or 1.5, for models 2 through 5.

The fluid (water) is simulated by assuming the following properties:

1. $E = 0.222 * 10^{10} Pa$ (Young's modulus)

2. $\rho = 0.1 * 10^4 kg / m^3$ (Density)

3. $\nu = 0.0$ (Poisson's Ratio)

The whole solid structure and fluid mesh was constructed using fifteen-node, three-dimensional isoparametric right triangular prismatic elements (PRIS15) from the ATILA finite element library [Ref.3].

ATILA offers monopolar, dipolar, and multipolar radiation boundary elements. Multipolar damping elements were selected to terminate the fluid mesh outer radius and the appropriate condition was set in the data input file.

The multipolar damping element used is a six-node isoparametric triangular element (TRIA06R) and it has to be spherical and attached to the outer surface of the fluid mesh.

The topology of the prismatic (PRIS15) and of the triangular (TRIA06R) elements are shown in Figures 3 and 4, respectively. The numbers represent the nodes and the order of numbering required for each element.

C.   MESH GENERATION

The major limitation of the three-dimensional finite element model is the number of degrees of freedom (D.O.F.) available (displacement along the coordinate axes, rotation along the coordinate axes, pressure, electric or magnetic potential, and magnetic excitation currents). For this reason the models developed were limited by the number of nodes and elements that were allowed.

Specifically, the number of nodes employed in the models ranged from 1546 to 2346 for the structure and fluid mesh, and the total number of elements ranged from 216 to 360. Of these, 144 to 288 are fluid elements and 72 are damping elements. The fluid mesh is arranged in successive layers of various thicknesses. The original fluid mesh was divided into four layers, two of them with 0.25m thickness and the other two fluid layers with 0.5m thickness.

Figure 5 shows a Mercator projection of the nodes and elements on the inner surface of the fluid. The node numbers and selected element numbers corresponding to this layer are given.

For the mesh generation procedure all the nodes were specified using spherical coordinates with the origin at the center of the spherical structure. The mesh spacing was always less than a quarter of the acoustic wavelength used.

The aspect ratio of each element according to the reference manual should be less than or equal to 3; in our models it is 1 to 4.
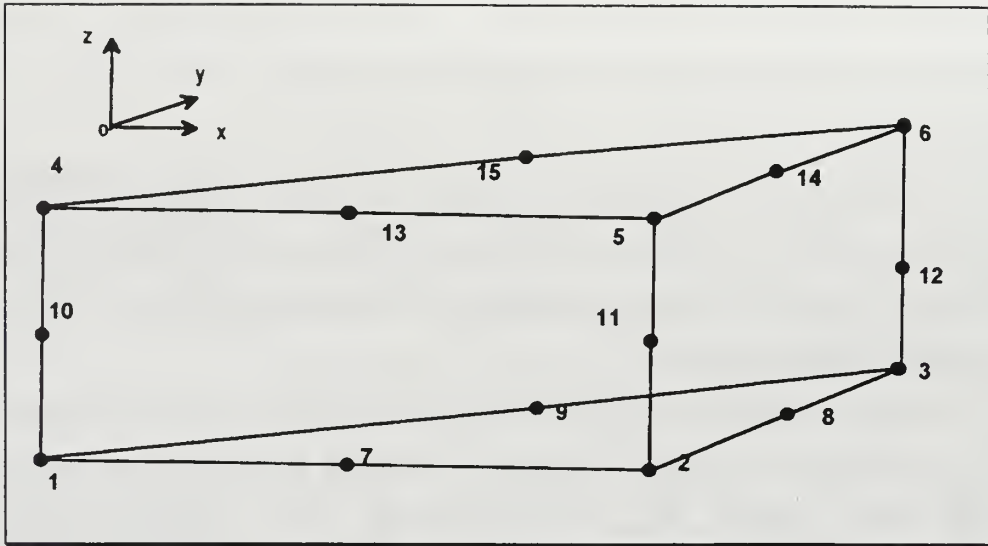
Figure 3. PRIS15F Element Topology. After Ref.[3]
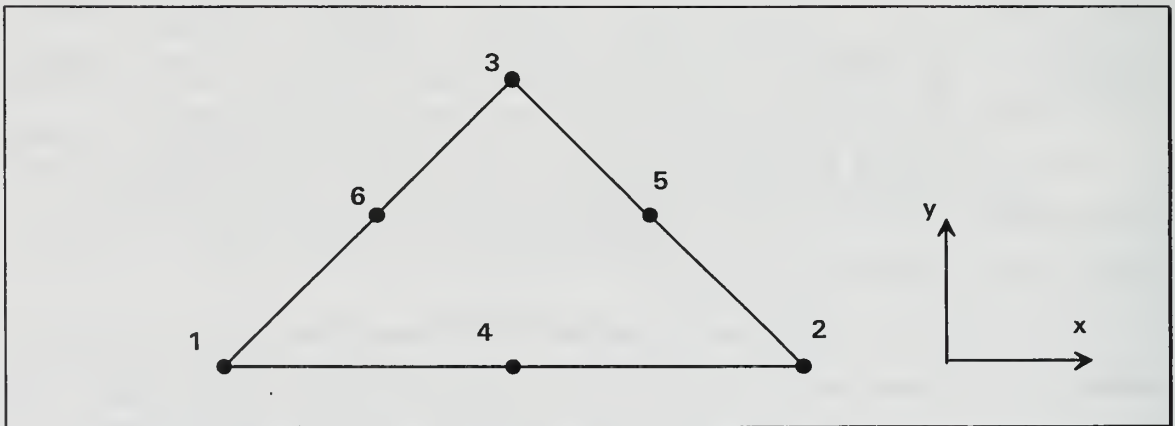
Figure 4. TRIA06R Element Topology. After Ref.[3]

12
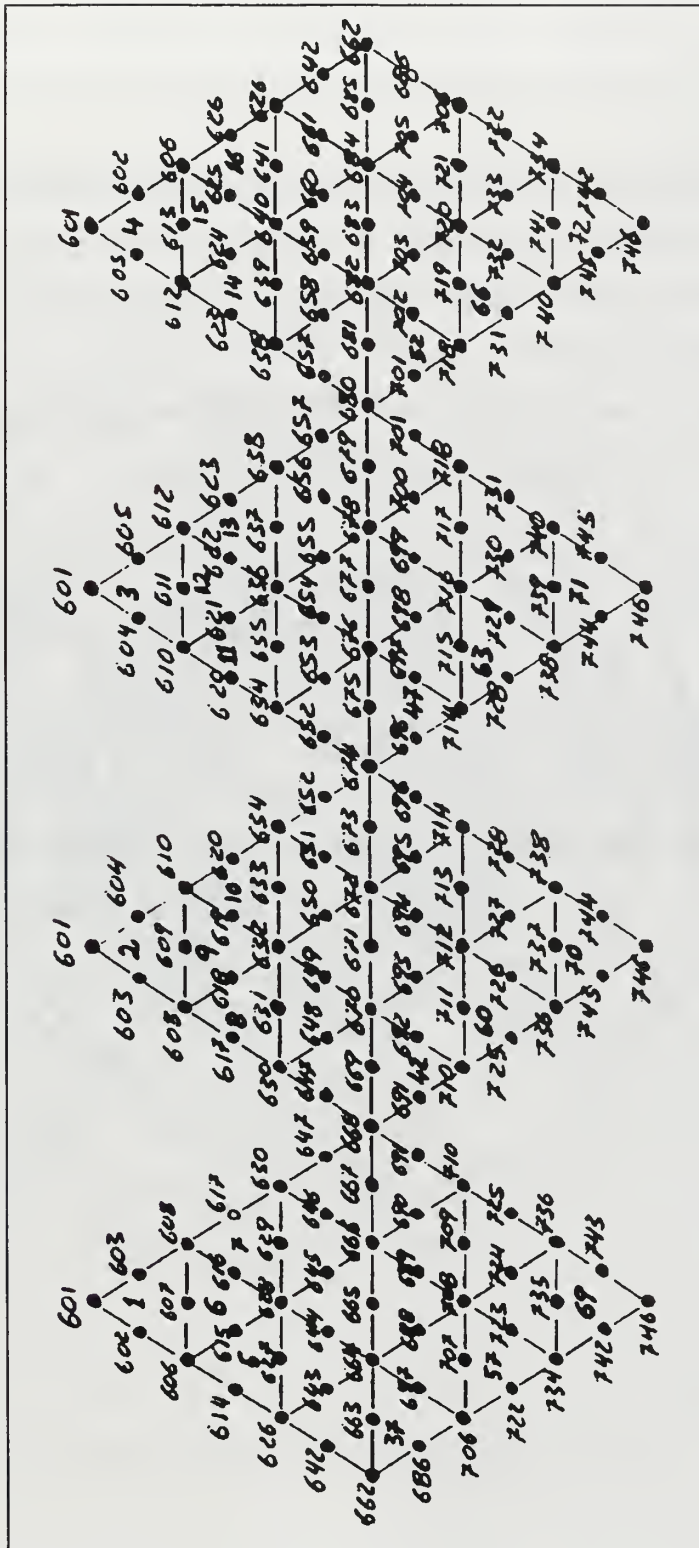
Figure 5. Inner Surface Fluid Layer Model, Mercator Projection.

13

The internal angles of our elements were modeled between 30 and 90 degrees while the reference manual states that these should lie between 30 and 100 degrees.

The mesh was built in such a way that adjacent elements, like elements 1 and 2 shown in Figure 5, were able to share common nodes. The top side exploded mesh view of the three dimensional model created by ATILA DEPL program is shown in Figure 6.

The types of isoparametric elements used in the mesh generation are described in [Ref. 3] and listed in the following Table 2.

Region	Element	Geometry
Fluid	PRIS15F	15-node triangular prism
Radiation Damping	TRIA06R	6-node triangular

Table 2. Isoparametric Elements Used in The Three Dimensional Mesh Generation
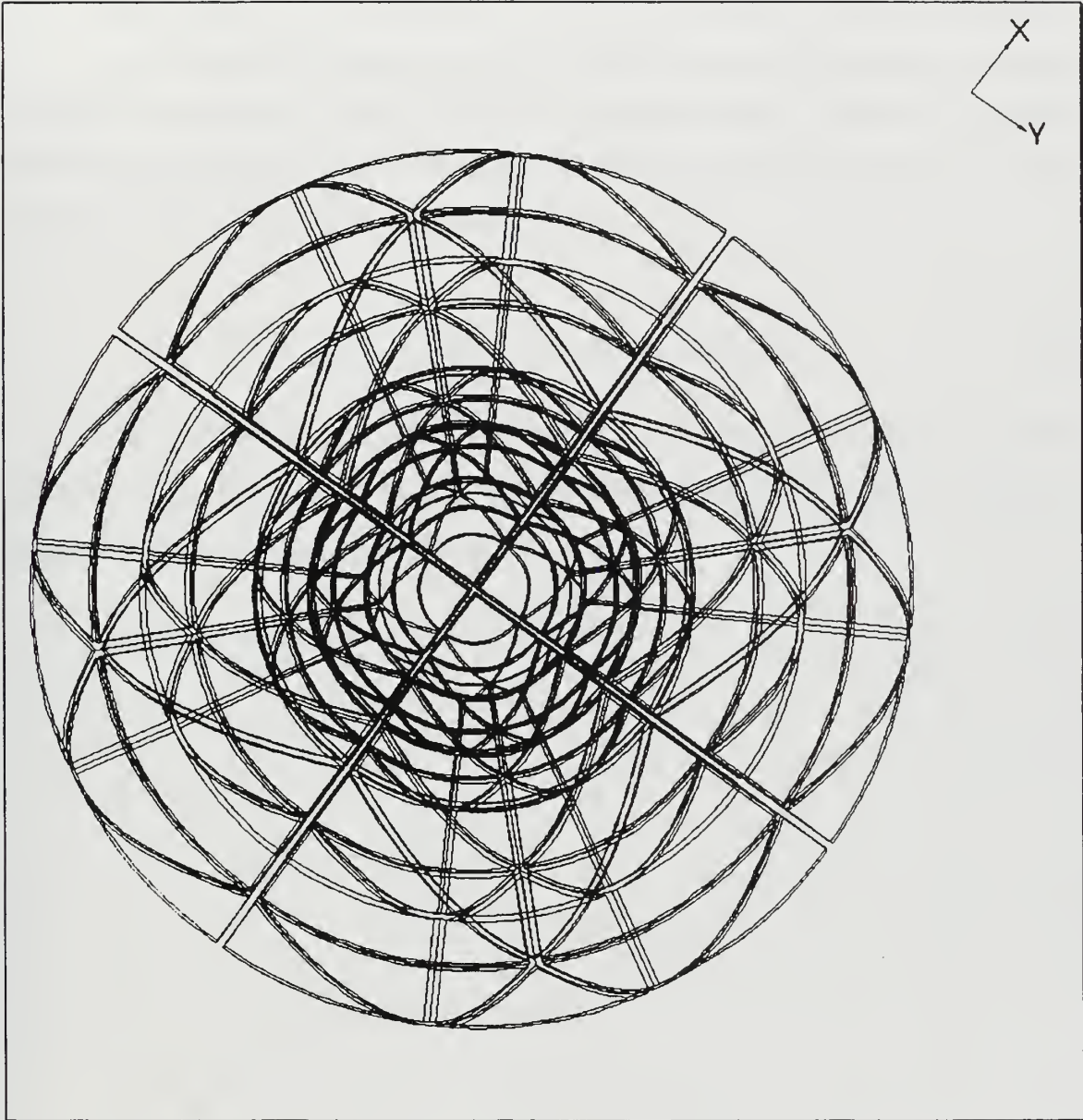
Figure 6. Three Dimensional Spherical Model. Topside View

IV. RESULTS

A.   EXACT ANALYTICAL RESULTS FOR SCATTERED PRESSURE WAVE

The linearized homogenous wave equation for the propagation of sound in ideal (nonviscous) fluids and the time-independent, lossless Helmholtz equation for a pressure wave with time-harmonic dependence $p(t,\underline{r}) = p(\underline{r}) * e^{j\omega t}$, at a position $\underline{r} = (r, \theta, \varphi)$ and time (t), is given by [Refs. 9, 10] :

$$\nabla^2 p(t,\underline{r}) - \frac{1}{c^2} \frac{\partial^2 p(t,\underline{r})}{\partial t^2} = 0 \Rightarrow \nabla^2 p(\underline{r}) + k^2 p(\underline{r}) = 0 \tag{1}$$

The solution of the Helmoltz Equation (1) for the incident (P_{in}) and scattered (P_{sc}) pressure fields in the spherical coordinate system shown in Figure 7 is given by Equations 2 and 3:
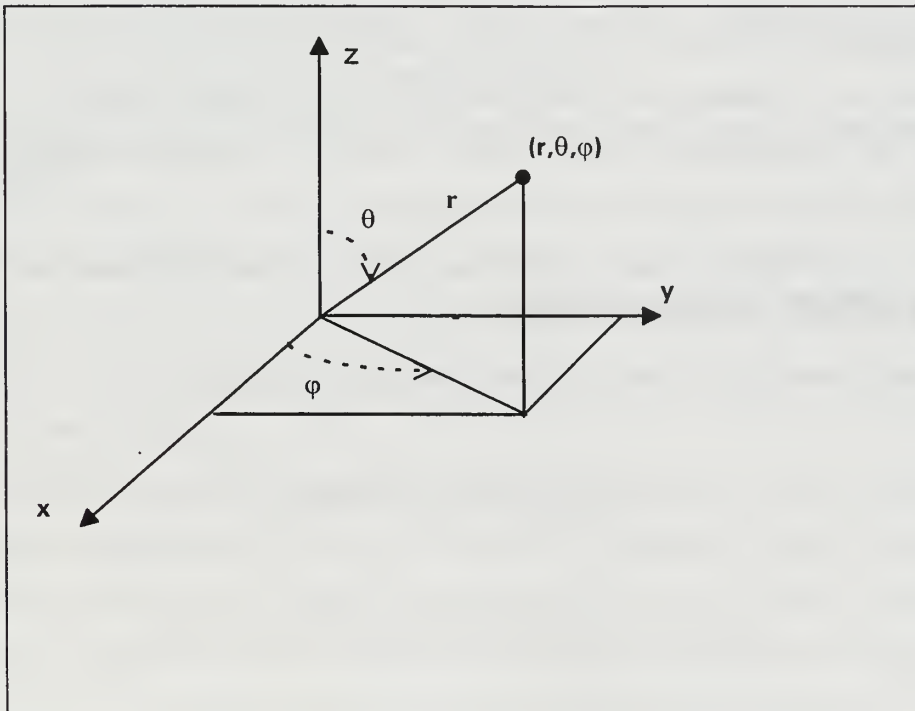
Figure 7. The Spherical Coordinates (r, θ, φ).

$$P_{in}(r,\theta,\varphi) = \sum_{n=0}^{\infty} \sum_{m=-n}^{n} P_{nm1} \cdot h_n^{(1)}(kr) \cdot Y_n^m(\theta,\phi) \tag{2}$$

$$P_{sc}(r,\theta,\varphi) = \sum_{n=0}^{\infty} \sum_{m=-n}^{n} P_{nm2} \cdot h_n^{(2)}(kr) \cdot Y_n^m(\theta,\phi) \tag{3}$$

where:

P_{nm1} and P_{nm2} are the amplitudes of the n,m components of the incident and scattered waves, respectively,

$h_n^{(1)}(kr)$ = the nth order spherical Hankel function of the first kind,

$h_n^{(2)}(kr)$ = the nth order spherical Hankel function of the second kind,

$Y_n^m(\theta,\phi)$ = the spherical harmonic of order n,m, which is related to the associated Legendre polynomial by the equation

$$Y_{nm}(\theta,\phi) = \sqrt{\frac{2n+1}{4\pi} * \frac{(n-m)!}{(n+m)!}} \cdot P_n^m(\cos\theta) \cdot e^{im\phi} .$$

Application of boundary conditions on the inner surface of the spherical fluid mesh for vanishing of the pressure or its normal derivative, provides solutions for the scattered wave for the case of a pressure release or rigid surface.

1. Analytical Expression for the Scattered Pressure from a Pressure Release Spherical Surface

The following equations apply for the n,m component:

$$P_{in}(r,\theta,\varphi) = Y_n^m(\theta,\varphi) \cdot h_n^{(1)}(kr) \tag{4}$$

$$P_{sc}(r,\theta,\varphi) = [-h_n^{(1)}(ka) / h_n^{(2)}(ka)] \cdot Y_n^m(\theta,\varphi) \cdot h_n^{(2)}(kr) \tag{5}$$

18

where:

a = the radius of the spherical shell,

k = the wavenumber of sound,

2. Analytical Expression for the Scattered Pressure from a Rigid Spherical Surface

The following equations apply:

$$P_{in}(r,\theta,\varphi) = Y_n^m(\theta,\varphi) \cdot h_n^{(1)}(kr) , \tag{6}$$

$$P_{sc}(r,\theta,\varphi) = [-\left(h_n^{(1)}(ka)\right)' / \left(h_n^{(2)}(ka)\right)'] \cdot Y_n^m(\theta,\varphi) \cdot h_n^{(2)}(kr) , \tag{7}$$

where $(h_n^{(1)}(ka))'$ and $(h_n^{(2)}(ka))'$ are the spatial derivatives of $h_n^{(1)}(kr)$ and $h_n^{(2)}(kr)$ evaluated at the spherical surface.

Appendix A contains a C program used to calculate analytically the values of the pressure scattered/radiated from a vibrating, spherically symmetric surface, for the above boundary conditions [Ref. 11].

B. NORMALIZED SCATTERED PRESSURE DEVIATION COMPUTED BY ATILA

Using the requried ATILA input data file, the pressure scattered by a rigid spherical surface due to an incident spherical harmonic wave was computed. The results were compared with an exact analytical solution computed using the C program described in Appendix A. Accordingly, the limitations of the boundary elements were obtained.

Since the scattered pressure is proportional to the incident pressure and has angular dependence, the error in the ATILA results at each finite-element node was quantified by normalizing the deviation from the exact value by the maximum magnitude of the scattered pressure at the same radius. This represents the normalized scattered pressure deviation computed by ATILA.

C. RESULTS FOR THE THREE DIMENSIONAL SPHERICAL MODEL (MODEL 1)

The following Figures 8 and 9 depict the results of the calculation for the original three-dimensional spherical model (model 1) that had been used in the previous investigation [Ref. 2]. In this model, the fluid is divided into four layers of thickness:

1.   Layer a: 0.25 m
2.   Layer b: 0.25 m
3.   Layer c: 0.5 m
4.   Layer d: 0.5 m

The radius of the scattering (inner) surface (a) is 0.5m: the radius of the radiation boundary is 2.0m. The frequency (f) is 474Hz; the corresponding wavenumber of sound in the water is $k = \frac{\omega}{c} = 2m^{-1}$.

Figure 8, from top to bottom, presents the normalized scattered pressure deviation computed by ATILA using multipolar dampers for monopolar and dipolar incident pressure fields, versus the dimensionless radius (kr) from the center of the structure. Figure 9 presents the normalized scattered pressure deviation for the quadrupolar incident pressure field.

The following Table 3 provides the normalized maximum error in percentages in the middle of each fluid layer and the angular location of that error for the monopolar, dipolar, and quadrupolar incident fields.

Nodes located at the poles are points with coordinate spherical angles: θ (polar) = 000,180 and φ (azimuthal) = 000, degrees. Nodes located on the equator are points with coordinate spherical angles: θ (polar) = 090 and φ (azimuthal) = 000,090,180,270 degrees. Near the equator, nodes are points with coordinate spherical angles: θ (polar) = 075,105 and φ (azimuthal) = 090,180,270 degrees.

NORMALIZED SCATTERED PRESSURE DEVIATION
COMPUTED BY ATILA USING MULTIPOLAR DAMPERS

MONOPOLAR RADIATION
n=0 / m=0

DIPOLAR RADIATION
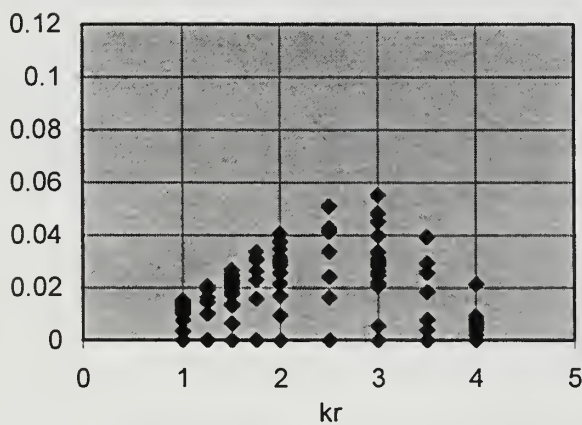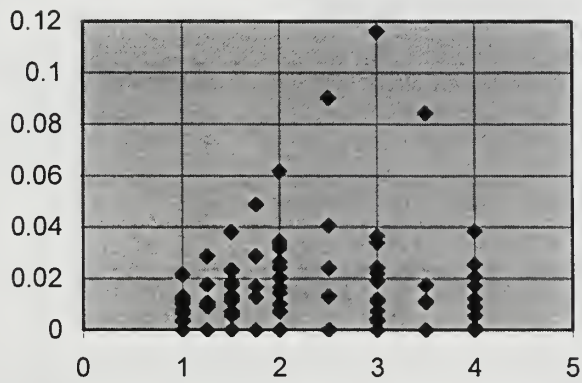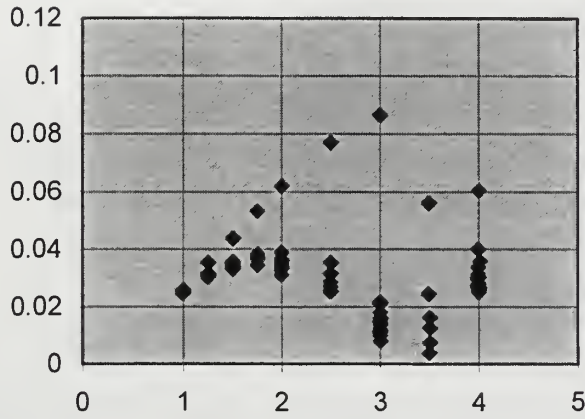n=1 / m=0

DIPOLAR RADIATION
n=1 / m=±1

Figure 8. Normalized scattered pressure deviation computed by ATILA versus kr for monopolar and dipolar incident fields.
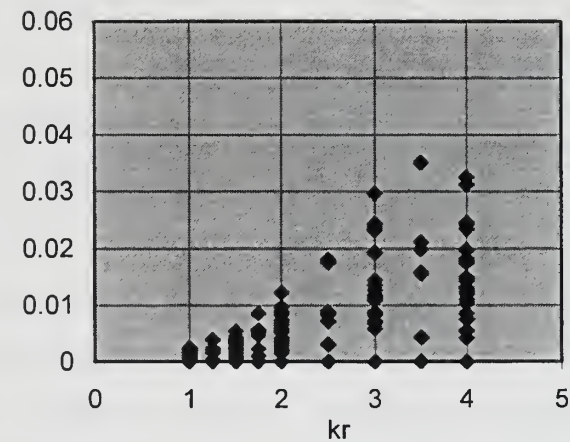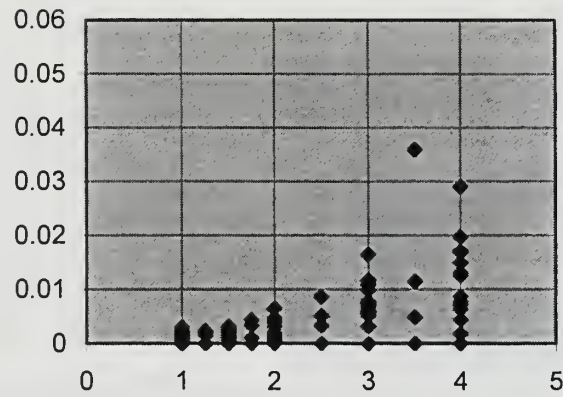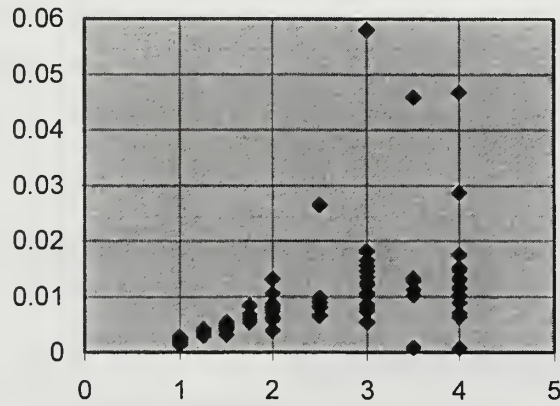
Figure 9. Normalized scattered pressure deviation computed by ATILA versus kr for quadrupolar incident field.

Type of Field	Scatterer Surface ka=1.0	Center of Layer a kr=1.25	Center of Layer b kr=1.75	Center of Layer c kr=2.5	Center of Layer d kr=3.5	Maximum Normalized Error	kr=1.5
Monopolar m=n=0	2.6 Poles	3.8 Poles	5.7 Poles	7.8 Poles	5.8 Poles	8.6 kr=3.0 Poles	4.6 Poles
Dipolar n=1, m=0	2.2 Poles	3.0 Poles	5.0 Poles	9.2 Poles	8.5 Poles	11.8 kr=3.0 Poles	3.9 Poles
Dipolar n=1, m=±1	1.8 Equator	2.2 Equator	3.6 Equator	5.1 Equator	4.0 Equator	5.7 kr=3.0 Equator	3.0 Equator
Quadrupolar n=2, m=0	0.3 Poles	0.4 Poles	0.8 Poles	2.7 Poles	5.3 Poles	5.8 kr=3.0 Poles	0.6 Poles
Quadrupolar n=2, m=±1	0.3 Equator	0.4 Equator	0.5 Equator	0.9 Equator	3.7 Equator	3.6 kr=3.5 Equator	0.5 Equator
Quadrupolar n=2, m=±2	0.3 Near Equator	0.5 Near Equator	0.9 Near Equator	1.9 Near Equator	3.6 Near Equator	3.6 kr=3.5 Near Equator	0.5 Near Equator

Table 3. Percent normalized scattered pressure deviation and location of the maximum error for monopolar, dipolar and quadrupolar incident fields.

From the above table and Figures 8 and 9, it can be concluded that:

1. The greatest normalized errors appear for the following type of fields:

a.   Monopolar, n=m=0: 8.6% at kr=3.0

b.   Dipolar, n=1, m=0: 11.8% at kr=3.0

c.   Quadrupolar, n=2, m=0: 5.8% at kr=3.0

2. For the above axisymetrical incident pressure fields the corresponding location of the maximum error points is close to the poles and exactly on the poles for the scatterer's surface and on the poles for each layer, respectively.

3.   For the cases, where the maximum error points appear on the equator or near the equator (dipolar n=1, m=±1, quadrupolar n=2, m=±1), the location of the minimum error points is on the poles.

4.   If the maximum error points are ignored for the monopolar and dipolar fields then the maximum normalized error is always less than 4%.

5.   If the maximum error points are ignored for the quadrupolar field then the maximum normalized error is always less than 3.5%.

6.   The normalized scattered pressure deviation computed by ATILA as it is presented in Figures 8 and 9 appears to increase when moving further away from the acoustic center.

The above results for the monopolar, dipolar and quadrupolar incident fields indicate that, for a given value of n, the maximum normalized errors occur for the axially symmetric type of fields (i.e., for m = 0). Hence, in investigating the influence of the fluid mesh inner radius (ka), the element's size (kL), and the fluid mesh outer radius (kR) on the results, only the axially symmetric incident waves were analyzed.

D.   INFLUENCE OF FLUID MESH INNER RADIUS

In order to evaluate the influence of fluid mesh inner radius on the results, models 2 and 3 were used. Recall that model 2 is divided into four equal fluid layers of thickness L=0.5m and the scatterer's radius is 0.5m. Model 3 is divided into three equal fluid layers of thickness L=0.5m and scatterer's radius 1.0m. For both cases, the radiation boundary and element's size satisfy kR=2.5 and kL=0.5, with k = 1.0m^{-1} and R=2.5m.

Figure 10 presents the influence of the scatterer's radius (ka) on the normalized scattered pressure deviation, versus kr. The monopolar (a,b), dipolar (c,d) and quadrupolar (e,f) fields are shown from top to bottom. On the left side the scatterer radius is ka=0.5 and on the right side the scatterer radius is ka=1.0.
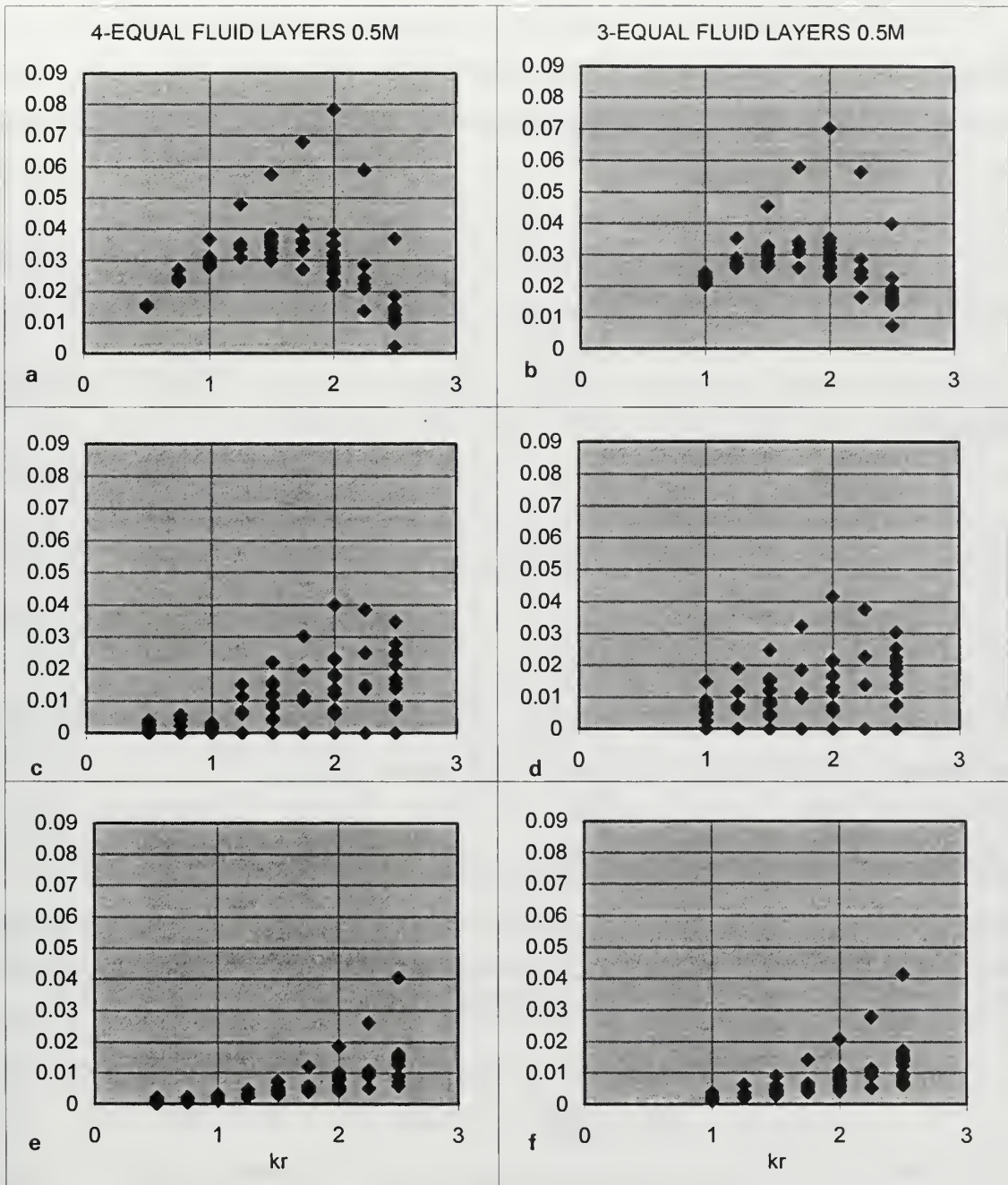
Figure 10. Normalized scattered pressure deviation computed by ATILA versus kr. From top to bottom monopoloar (a,b), dipolar (c,d) and quadrupolar (e,f) incident field; on the left: scatterer radius ka = 0.5; on the right: scatterer radius ka = 1.0, radiation boundary R and element size L satisfy: kR = 2.5 and kL = 0.5 for all cases.

Table 4 summarizes the results for the maximum error in percent in the middle of each layer and the node location for the monopolar, dipolar and quadrupolar incident fields when the scatterer radius ka varies and kL and kR do not.

Type of Field	Scatterer Surface	Center of Layer a kr=0.75	Center of Layer b kr=1.25	Center of Layer c kr=1.75	Center of Layer d kr=2.25	Maximum Normalized Error	kr=1.5
Monopolar n=m=0	Poles	Poles	Poles	Poles	Poles	Poles	Poles
ka=1.0	2.4	----	3.5	5.8	5.7	7.0 kr=2.0	4.6
ka=0.5	1.7	2.9	4.9	6.9	5.9	7.8 kr=2.0	5.7
Dipolar n=1, m=0	Poles	Poles	Poles	Poles	Poles	Poles	Poles
ka=1.0	1.5	----	1.9	3.3	3.8	4.2 kr=2.0	2.5
ka=0.5	0.5	0.6	1.8	3.0	3.9	4.0 kr=2.0	2.2
Quadrupolar n=2, m=0	Poles	Poles	Poles	Poles	Poles	Poles	Poles
ka=1.0	0.4	----	0.6	1.4	2.8	4.1 kr=2.5	0.9
ka=0.5	0.2	0.3	0.5	1.2	2.6	4.1 kr=2.5	0.7

Table 4. Percent normalized scattered pressure deviation and location of the maximum error for monopolar, dipolar and quadrupolar incident pressure field when ka=1.0 and ka=0.5, radiation boundary kR=2.5, element's size kL=0.5.

From this table and Figure 10 it is observed that:

1.   For the monopolar field:

a.   The normalized error at a given value of kR decreases as ka is increased from 0.5 to 1.0.

b.   The maximum error decreases as the scatterer radius ka is increased from 0.5 (7.8%) to 1.0 (7.0%).

c.   For both cases, the maximum error occurs at kR=2.0.

d.   If the maximum error points (poles) are disregarded, then the maximum error is less than or equal to 4%.

26

2.   For the dipolar field:

a.   The normalized error at kr = 1.0 increases by a factor of 5, from about 0.3% to about 1.5% as the scatterer radius ka is increased from 0.5 to 1.0.

b.   The normalized error at all other radii is essentially unchanged by varying ka.

c.   The maximum error still occurs at kr=2.0 as it occurred for the monopolar field.

d.   When the maximum error points (poles) are disregarded then the maximum error is less than 3%.

3.   For the quadrupolar field:

a.   The normalized error at a given node shows very little dependence on the value of ka.

b.   The maximum error remains the same (4.1%) as the scatterer radius ka is increased from 0.5 to 1.0, from the acoustic center

c.   For both cases, if the maximum error points are disregarded then the error is less than 2%.

For the above dipolar and quadrupolar fields, the minimum error appears on the equatorial points. Moreover, from Figure 10, very similar deviation curves for the monopolar (a,b), dipolar (c,d) and quadrupolar (e,f) fields, for ka=0.5 and ka=1.0 are observed. Also, we observe that the maximum normalized error on the scatterer's surface increases as the scatterer's radius increases.

E.   INFLUENCE OF FLUID MESH ELEMENT SIZE

In order to evaluate the influence of fluid mesh element size on the results, we used models 2 and 4. Recall that model 2 is divided into four equal fluid layers of thickness L=0.5m while model 4 is divided into two equal fluid layers of thickness L=1.0m. For both cases, the radiation boundary and scatterer's radius satisfy kR=2.5 and ka=0.5, with $k = 1.0m^{-1}$, R=2.5m and a=0.5m.

Figure 11 presents the influence of the element's size (kL) on the normalized scattered pressure deviation, versus kr. The monopolar (a,b), dipolar (c,d), and quadrupolar (e,f) fields are shown from top to bottom. On the left side the element's size is kL=0.5 and on the right side the element's size is kL=1.0.

Table 5 summarizes the results for the maximum error in percent on the scatterer's surface, in the middle and at the end of each layer and the node location for the monopolar, dipolar and quadrupolar fields, when the element's size varies and kR, ka do not.

Type of Field	Scatterer Surface ka=0.5	kr=1.0	kr=1.5	kr=2.0	kr=2.5	Maximum Normalized Error	kr=1.5
Monopolar n=m=0	Poles	Poles	Poles	Poles	Poles	Poles	Poles
kL=1.0	1.2	4.1	6.3	6.3	4.5	6.3 kr=2.0	6.3
kL=0.5	1.7	3.8	5.7	7.9	3.8	7.9 kr=2.0	5.7
Dipolar n=1, m=0	Poles	Poles	Poles	Poles	Poles	Poles	Poles
kL=1.0	0.7	1.0	2.6	3.3	3.9	3.9 kr=2.5	2.6
kL=0.5	0.6	0.5	2.2	4.0	3.6	4.0 kr=2.0	2.2
Quadrupolar n=2, m=0	Poles	Poles	Poles	Poles	Poles	Poles	Poles
kL=1.0	0.2	0.6	0.9	1.7	4.2	4.2 kr=2.5	0.9
kL=0.5	0.2	0.6	0.7	1.9	4.0	4.0 kr=2.5	0.7

Table 5. Percent normalized scattered pressure deviation and location of the maximum error, for monopolar, dipolar and quadrupolar incident pressure field, when kL=1.0 and kL=0.5, scatterer radius ka=0.5, radiation boundary kR=2.5.
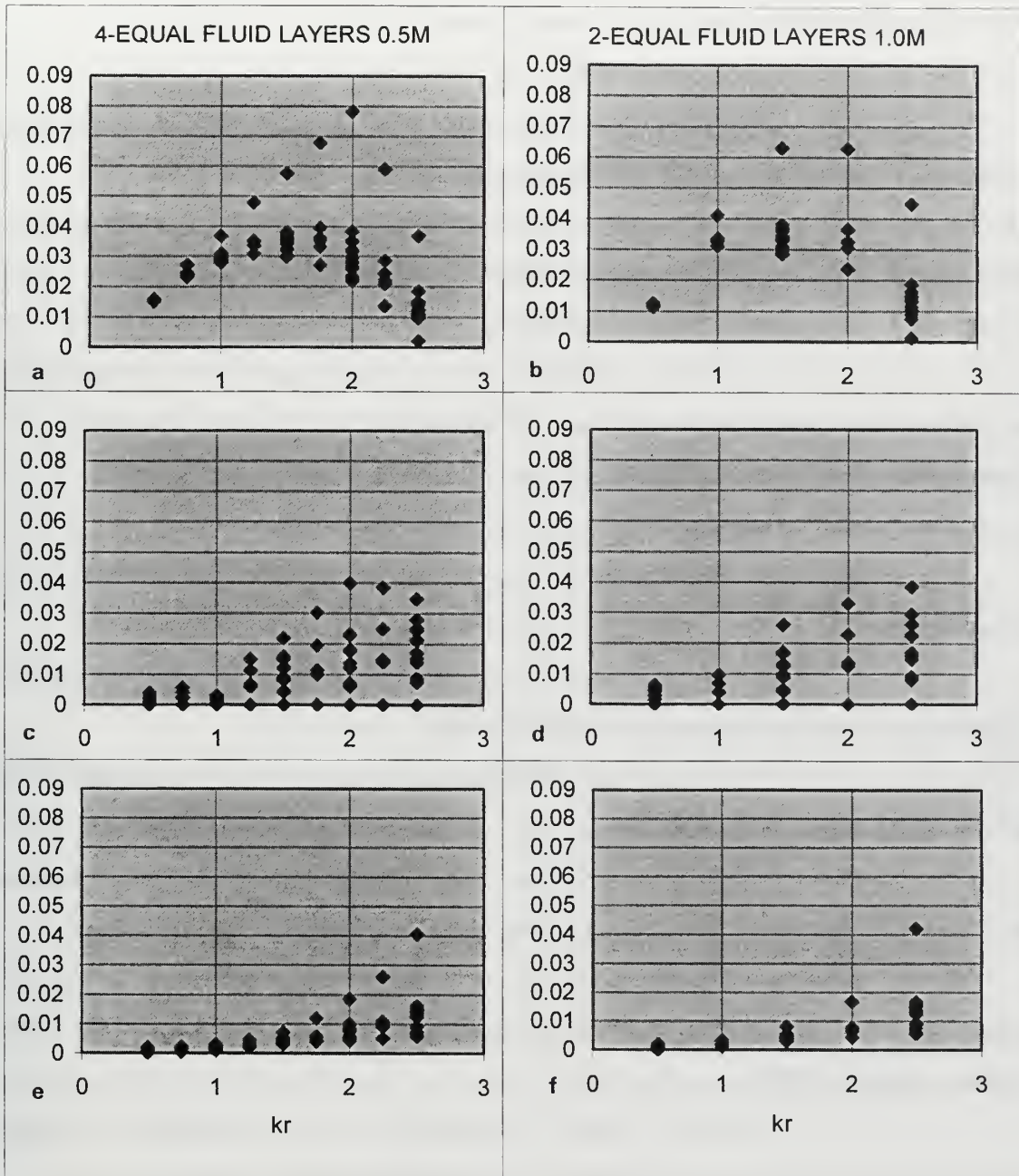
Figure 11. Normalized scattered pressure deviation computed by ATILA versus kr. From top to bottom monopolar (a,b), dipolar (c,d) and quadrupolar (e,f) incident field; on the left: element size kL = 0.5: on the right: element size kL = 1.0. Scatterer radius a and radiation boundary R satisfy: ka = 0.5 and kR = 2.5 for all cases.

From this table and Figure 11 we observe that:

1. For the monopolar field:

  a. On the scatterer's surface ka=0.5, as the element's size is increased, the maximum error decreases slightly from 1.7% to 1.2%.

  b. The maximum error at each layer becomes greater as kL is increased, except at the maximum deviation point, at kr=2.0.

  c. For both cases the maximum error occurs at kr=2.0.

  d. Once the maximum error points (poles) are disregarded, then the maximum error is less than or equal to 4%. Also, in that case, the corresponding deviation for both cases is similar.

2. For the dipolar field:

  a. On the scatterer's surface for both cases the deviation is almost the same.

  b. As the element's size is increased, the error increases except at the maximum deviation point at kr=2.0.

  c. The maximum deviation for kL=0.5 occurs at kr=2.0, while for kL=1.0 it occurs at kr=2.5.

  d. When the maximum error points (poles) are disregarded, then the maximum deviation is very similar and less than 3% for both cases.

3. For the quadrupolar field:

  a. On the scatterer's surface, ka=0.5, the maximum deviation for both cases is 0.2%.

  b. For both cases, the variation in the normalized deviation follows the same trend, and corresponding values are very close to each other.

  c. For both cases, when the maximum error points are disregarded, the deviation is less than 2%.

  d. The maximum deviation occurs at kr=2.5 for both cases.

F. INFLUENCE OF FLUID MESH OUTER RADIUS

In order to evaluate the influence of the mesh outer radius, we used models 2 and 5. Model 2 is the reference model and is divided into four equal

fluid layers of thickness L=0.5m, while model 5 is divided into two equal fluid layers of thickness L=0.5m. For both cases, the scatterer radius a and elements size L, satisfy ka=0.5 and kL=0.5, for $k = 1.0m^{-1}$ and a=0.5m.

Figure 12, presents the influence of the radiation boundary (kR) on the normalized scattered pressure deviation versus kr. The monopolar (a,b), dipolar (c,d) and quadrupolar (e,f) fields are shown from top to bottom. On the left side the radiation boundary is kR=1.5 and on the right side the radiation boundary is kR=2.5.

Table 6 summarizes the results for the maximum error in percent in the middle of each layer and the node location for the monopolar, dipolar and quadrupolar fields when the radiation boundary kR varies and kL and ka are the same.

It is observed from this table and Figure 12 that :

1.   For the monopolar field:

        a.   At a given radius, the error increases as the radiation boundary kR is increased. For example, in the case where kR=2.5, the error is 100% greater than the corresponding error when kR=1.5 at the location where kr=1.5.

        b.   At the outer fluid boundary, the error remains almost the same (2%) when the maximum error points (poles) are disregarded.

        c.   When kR=1.5, the maximum error occurs at the outer radius surface points. On the other hand, when kR=2.5, the maximum error occurs at kr=2.0.

2.   For the dipolar field:

        a.   The error decreases drastically as we increase the radiation boundary kR and becomes almost 100% lower at the boundary for kR=2.5.

        b.   The maximum error still occurs at the same radius as it does for the monopolar field.
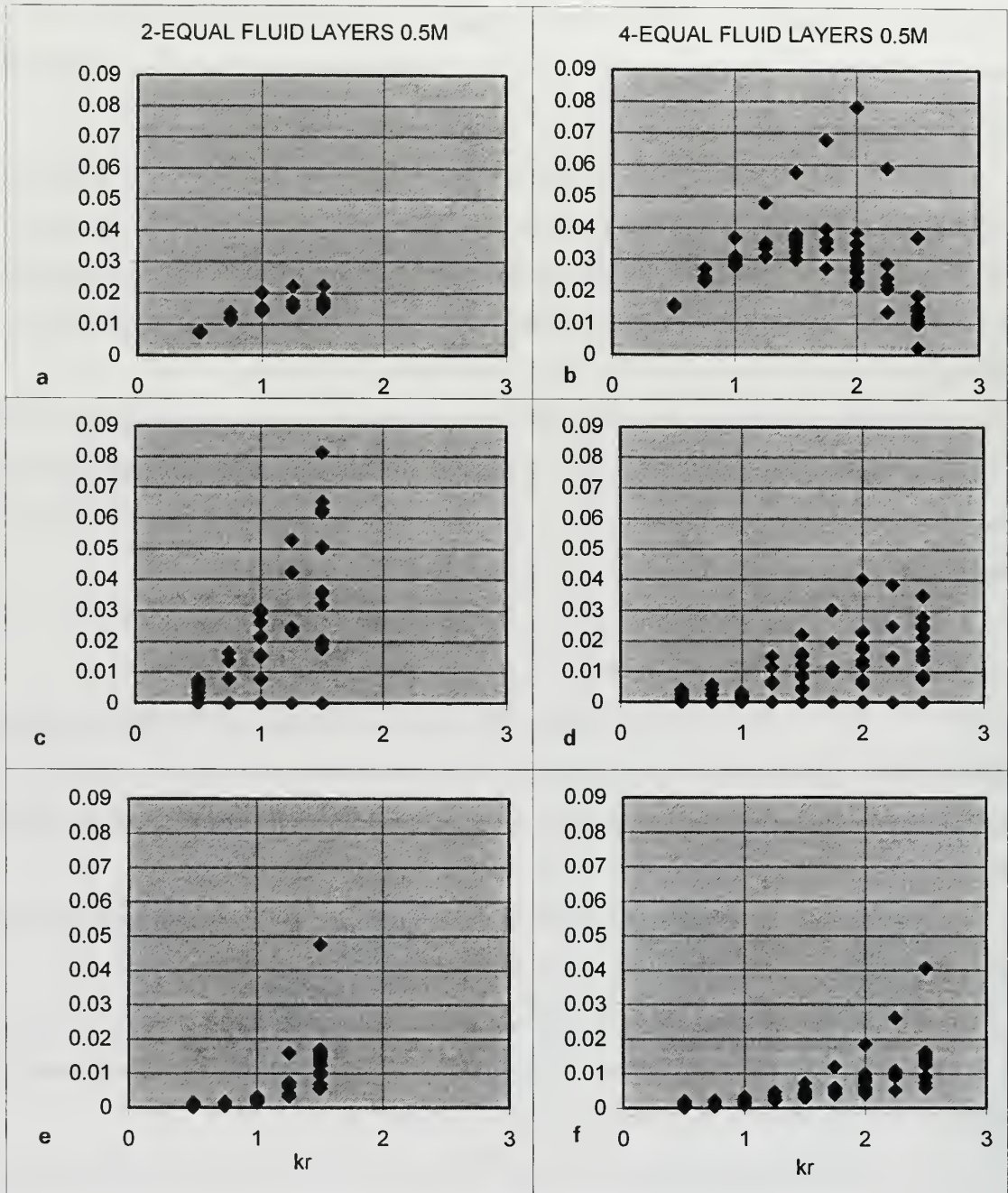
31

Figure 12. Normalized scattered pressure deviation computed by ATILA versus kr. From top to bottom monopolar (a,b), dipolar (c,d) and quadrupolar (e,f) incident field; on the left: radiation boundary at kR = 1.5; on the right: radiation boundary at kR = 2.5; scatterer radius a and element size L satisfy: ka = 0.5 and kL = 0.5 for all cases.

32

Type of Field	Scatterer Surface ka=0.5	Center of Layer a kr=0.75	Center of Layer b kr=1.25	Center of Layer c kr=1.75	Center of Layer d kr=2.25	Maximum Normalized Error	kr=1.5
Monopolar n=m=0	Poles	Poles	Poles	Poles	Poles	Poles	Poles
kR=1.5	0.8	1.4	2.3	----	----	2.3 kr=1.5	2.3
kR=2.5	1.7	2.9	4.9	6.9	5.9	7.8 kr=2.0	5.7
Dipolar n=1, m=0	Poles	Poles	Poles	Poles	Poles	Poles	Poles
kR=1.5	0.8	1.6	5.3	----	----	8.1 kr=1.5	8.1
kR=2.5	0.5	0.6	1.8	3.0	3.9	4.0 kr=2.0	2.2
Quadrupolar n=2, m=0	Poles	Poles	Poles	Poles	Poles	Poles	Poles
kR=1.5	0.2	0.2	1.6	----	----	4.8 kr=1.5	4.8
kR=2.5	0.2	0.3	0.5	1.2	2.6	4.1 kr=2.5	0.7

Table 6. Percent normalized scattered pressure deviation and location of the maximum error for monopolar, dipolar and quadrupolar incident fields, when kR=1.5 and kR=2.5, scatterer radius ka=0.5 and element size kL=0.5.

        c.   Once again, if we disregard the maximum error points (poles), for kR=2.5, the error is always less or equal to 3%. On the other hand, for kR=1.5, the error is less than 7%.

        d.   The minimum error points for both cases appear on the equator.

        3.   For the quadrupolar field:

        a.   At a given radius, the error decreases as the radiation boundary increases.

        b.   The maximum error for kR=1.5 and kR=2.5 occurs on the outer boundary surface.

        c.   For both cases, if the maximum error points (poles) are disregarded the error is always less than 2%.

d.   Finally, the minimum error for both cases appears on the equatorial points.

G.   SUMMARY OF RESULTS

The detailed analyses developed for the five models listed in Chapter III, Table 1, indicate that:

1.   For the original three dimensional model (model 1), the maximum deviation occurs close to or at the poles for the axially symmetric monopolar (8.6%), dipolar (11.8%) and quadrupolar (6%) incident pressure fields. Also, the minimum deviation points are at equatorial nodes. Moreover, for the non-axially symmetric incident fields, the maximum deviation is less than 5.5% and occurs at equatorial points, while the minimum deviation occurs at points located at the poles.

2.   Further investigation of the influence of the fluid mesh inner radius (ka), the element's size (kL), and the fluid mesh outer radius (kR), on the results for axially symmetric incident pressure fields, revealed that:

a.   For monopolar and dipolar incident fields, when the poles are disregarded:

(1)   As the radiation boundary kR increases while ka and kL remain constant, the maximum deviation decreases by approximately the same amount in percent. This occurs specifically from 6.6% when kR=1.5, to 4% when kR=2.5, for ka=0.5 and kL=0.5, respectively, which corresponds to 65%.

(2)   As the scatterer's radius ka increases, while kL and kR remain constant, the maximum deviation decreases by a small amount in percent. This occurs, specifically, from 4% when ka=0.5, to 3.7% when ka=1.0, for kL=0.5 and kR=2.5, respectively, which corresponds to 8%.

(3)   As the element's size kL increases, while ka and kR remain constant, the maximum deviation remains constant.

b.   For a quadrupolar incident field, the maximum deviation remains essentially the same between 1.9% and 1.8%.

34

Table 7, which combines three tables, summarizes our results for the maximum normalized error in percent, when the poles are disregarded, and the type of field for which this error occurs. Also, from this table it can be observed that the maximum deviation occurs for monopolar and dipolar axially symmetric incident fields.

ka=0.5	kL=0.5	kL=1.0
kR 1.5	6.6 Dipolar	-------
kR 2.5	4.0 Monopolar	4.0 Dipolar

kL=0.5	ka=0.5	ka=1.0
kR 1.5	6.6 Dipolar	-------
kR 2.5	4.0 Monopolar	3.7 Monopolar

kR=2.5	kL=0.5	kL=1.0
ka=0.5	4.0 Monopolar	4.0 Dipolar
ka=1.0	3.7 Monopolar	-------

Table 7. Percent normalized maximum scattered pressure deviation and type of incident pressure field, when poles are disregarded, computed by ATILA.

V. CONCLUSIONS AND SUGGESTIONS FOR FURTHER INVESTIGATION

A.   CONCLUSIONS

Five three-dimensional spherical models were developed in order to evaluate the radiation boundary elements used in the ATILA finite element code. The models simulate a rigid spherical solid structure surrounded by an infinite fluid.

Monopolar, dipolar, and quadrupolar incident spherical pressure wave fields were imposed, and the scattered pressure was calculated using ATILA. Since the scattered pressure is proportional to the incident pressure and has angular dependence, the error in the ATILA results at each finite-element node was quantified by normalizing the deviation from the exact value by the maximum magnitude of the scattered pressure at the same radius.   This represents the normalized scattered pressure deviation computed by ATILA.

The range of values of the dimensionless lengths which characterized the problem was:

        The fluid mesh inner radius ka (scatterer radius): 2.0 , 1.0 , 0.5

        The fluid mesh element size kL: 0.5 , 1.0

        The radiation boundary kR: 4.0 , 2.5 , 1.5

The maximum deviations observed were for the axially symmetric monopolar (9%), dipolar (12%), and quadrupolar (6%) incident pressure fields. For these cases, it can be concluded that the maximum deviation points are at the poles, while the minimum deviation occurs on the equatorial points.

When the poles are disregarded, for the monopolar and dipolar incident pressure fields there is a strong influence of the fluid mesh outer radius (kR) and a weak influence of the fluid mesh inner radius (ka) on the results. Specifically, as the fluid mesh outer radius increases and/or the fluid mesh inner radius increases then the normalized scattered pressure deviation decreases. For the

quadrupolar field, the maximum deviation remains essentially constant, independent of the above factors (ka, kR). Furthermore, variation of the elements size (kL) does not affect the maximum normalized scattered pressure deviation.

Moreover, for the non-axially symmetric incident pressure fields, the maximum deviation observed was less than 5.5%, and was found to occur at nodes on the equator, while the minimum deviation points were located at the poles.

B.   SUGGESTIONS FOR FURTHER INVESTIGATION

The magnitudes of the errors in the scattered pressures computed by ATILA were larger than expected, based upon the mesh sizes employed in the models; for all of the models the radial length L of the fluid elements was less than 1/6 wavelength. It would have been desirable to examine the calculated scattering for a more refined mesh. However, to divide the element scale size by a factor of 2 would have resulted in models which exceed the allowed number of degrees of freedom. Of course, this is because all the models employed were fully three-dimensional, and did not make use of any possible reductions in size due to wave function symmetry (in fact, our choice of $e^{j\phi}$ for the azimuthal wave function precluded reduction in that direction). Also, we are interested in the computed scattering in all of the spherical harmonic wave components for an incident wave of only one component.

It is suggested that further investigation of the performance of the ATILA radiation boundary elements be conducted using two-dimensional models. It might also be advantageous to use $\sin\phi$ or $\cos\phi$ instead of $e^{jm\varphi}$ to represent the azimuthal dependence. This will allow a finer mesh to be employed, and a broader range of values of ka, kL, and kR to be examined.

APPENDIX A. C CODE FOR ANALYTICAL PRESSURE SCATTERED CALCULATION

```
***********************************************************************
* PROGRAM SCHAR.C , by Panagiotis Sinanoglou 2/2/1996
* Program:Computes the Scattered Spherical Harmonic pressure from a rigid
* spherical structure at the point r1(x,y,z), for the Wavenumber k, for:
* natural boundary and pressure release condition
* Input Variables:
*    x,y,z: Cartesian Coordinates of the Node Point.
*        k: Wavenumber.
*       r2: Radius of the Scatterer's Surface.
*      n,m: Orders of Spherical Hankel and Legendre functions.
* Output Variables:
*       r1: Radius in meters.
*      phi: Azimouthial angle in degrees.
*    theta: Polar angle in degrees.
*      rp5: Real part of computed scattered pressure at r1 in pascals
*      rp6: Imaginary part of computed scattered pressure   at r1 in pascals
* Formula for Incident Wave: Pinc=Pnm(costheta)*e^(imphi)*hn(1)(kr2)
* Formula for Scattered Wave from Rigid Boundary:
* Psc=-Pnm(costheta)*e^(imphi)*[hn'(1)(kr2)/hn'(2)(kr2)]*hn2(kr1)
* Formula for Scattered Wave from Pressure Release Surface:
* Psc=-Pnm(costheta)*e^(imphi)*[hn(1)(kr2)/hn(2)(kr2)]*hn2(kr1)
* External Functions: sphbes.c, plgndr.c, bessjy.c, beschb.c, chebev.c,
  complex.c, nrutil.c
* Header Files for prototype function declaration:nr.h nrutil.h,complex1.h
* Functions:
* Normalized Legendre[ plgndr(n,m,x) ],Spherical Hankel for the
* real and the imaginary parts[ sphbes(n,(k*r2),&xsj,&xsy,&xsjp,&xsyp) ],
* Complex(structures)[ Cexp(mphi), Cdiv(a,b), Cmul(a,b), RCmul(a,b) ]
* File nphra33n.c provides node coordinates(x,y,z).
* File dim1.dt stores the corresponding spherical coordinates(r1,theta,phi)
* File dim13.dt stores the Legendre plgndr(n,m,(z/r1).
* File dim11.dt stores the real,imaginary part of exp. function e^(imphi).
* File dim14.dt stores the ratio of the derivatives of the Spherical Hankel  for the
  real and
* imaginary part of hn'(1)(kr2)/hn'(2)(kr2) for natural boundary conditions and the
  ratio of
*hn(1)(kr2)/hn(2)(kr2) for pressure release,evaluated at the scattering surface, at
  r2=0.5m.
* File dim15.dt stores the real and the imaginary part of the Spherical
* Hankel hn2(kr1) at the node range r1.
```

* File dim16.dt stores the real and the imaginary part of the scattered pressure
  Psc, at the * range r1.
  ****

```c
#include <stdio.h>
#include <math.h>
#include<string.h>
#include<stdlib.h>
#include "complex1.h"
#define NRANSI
#include "nr.h"
#include "nrutil.h"
#define pi 3.141592654

main()
{
    FILE *f1; FILE *f3;  FILE *f2;   FILE *f4; FILE *f5;FILE *f6;FILE *f7;
    FILE *f20; FILE *f21;FILE *f22;
    fcomplex a,b,hn2;
    float r2=0.5,k=2.0;
    float sj,sy,sjp,syp,xsj,xsy,xsjp,xsyp,rp1,rp2,rp3,rp4,rp5,rp6;
    int j,rpm;
    float fac,val,t,f11,f12,f13,f14,Pnm,s1,s2;
    unsigned int factorial(unsigned int a);
    double x,y,z,z1,r,r1,theta,phi,q,mphi;
    int d,i,N,ch,m,n;
    char g[11],h[11],c[11],e[11],f[11];

    f3=fopen("dim1.dt","w");
    printf("Enter the integer valuesfor N,n,m\n");
    scanf("%d %d %d",&N,&n,&m);
    f4=fopen("sphra33b.c","r");
    f5=fopen("dim11.dt","w");
    f6=fopen("dim12.dt","w");
    f7=fopen("dim13.dt","w");
    f20=fopen("dim14.dt","w");
    f21=fopen("dim15.dt","w");
    f22=fopen("dim16.dt","w");
  for(i=0; i<N; ++i)
  {
    fscanf(f4,"%lf %lf %lf %d
%lf%s%s%s%s%s\n",&x,&y,&z,&d,&q,&g,&h,&c,&e,&f);
/* Converts from cartesian(x,y,z) to spherical coordinates(r1,theta,phi).*/
    if((x>0.0 &&  y>=0.0))
        { r1=sqrt(x*x+y*y+z*z);
```

```c
        phi=atan(y/x);
        theta=acos(z/r1);}
    else if(x==0.0 && y==0.0 && z==0.0)
        {r1=0.0; theta=0.0; phi=0.0;}
    else if (x==0.0 && y==0.0 && z!=0.0)
        { r1=sqrt(x*x+y*y+z*z);
         phi=0.0;
         r1=sqrt(x*x+y*y+z*z);
         theta=acos(z/r1);}
    else if(x==0.0 && y>0.0 &&(z==0.0||z!=0.0))
        { phi=pi/2;
         r1=sqrt(x*x+y*y+z*z);
           theta=acos(z/r1);}
     else if(y==0.0 && x<0.0 )
        { phi=pi;
          r1=sqrt(x*x+y*y+z*z);
           theta=acos(z/r1);}
    else if(y<0.0 && x==0.0)
       { phi=3*(pi/2);
          r1=sqrt(x*x+y*y+z*z);
           theta=acos(z/r1);}
     else if ((x<0.0 && y>0.0) )
       {phi=+(pi)+atan(y/x);
          r1=sqrt(x*x+y*y+z*z);
           theta=acos(z/r1); }
   else if (x<0.0 && y<0.0)
       { phi=pi+atan(y/x);
          r1=sqrt(x*x+y*y+z*z);
           theta=acos(z/r1);}
     else if (x>0.0 && y<0.0)
       { phi=(2*pi)+atan(y/x);
          r1=sqrt(x*x+y*y+z*z);
           theta=acos(z/r1);}

    theta=theta*(180/pi);
    phi=phi*360/(2*pi);
    fprintf(f3,"  %+4.3lf  %+6.3lf  %+6.3lf\n",r1,(theta),(phi));

/* The required value of xx=cos(theta) for the Pnm(xx) is: (z/r1) */
/* Calculates the Normalized Legendre function "plgndr(n,m,(z/r1) */
   fprintf(f7,"%4s %4s %10s  %24s\n","n","m","x","plgndr(n,m,x)");
rpm=abs(m);
            if( m>=0  )
          { f13=factorial(n-m);
             f14=factorial(n+m);
```

41

```c
            s1=sqrt((2*n+1)*f13/(4*pi*f14));
            Pnm=(plgndr(n,m,(z/r1))*s1);
                        fprintf(f7,"%4d %4d %13.6lf  %19.6e\n",n,m,(z/r1),Pnm);
            }
        if(m<0)
         { f13=factorial(n-rpm);
           f14=factorial(n+rpm);
           s2=sqrt((2*n+1)*f14/(4*pi*f13));
           f11=factorial(n-rpm);
           f12=factorial(n+rpm);
           r=pow(-1,rpm);
           t=r*(f11/f12);
           Pnm=(plgndr(n,rpm,(z/r1))*t*s2);
  fprintf(f7,"%4d %4d %13.6lf %19.6e\n",n,m,(z/r1),Pnm);
            }
/* Calculates the e^(imphi) Real/Imagin parts */

    mphi=(m*phi)*2*(pi/360);
    fprintf(f6,"%lf  %lf \n",Cexp(mphi).r,Cexp(mphi).i);
/* Calculates the (z/r1),phi(degrees) */
    fprintf(f5,"%+6.3lf  %+6.3lf \n",(z/r1),(phi));
/* Calculates the ratio of the Spherical Hankel for the real and the imaginary
parts    */
/* of  hn'(1)(kr2)/hn'(2)(kr2) on the scattering surface at r2=0.5 for  N.B.C , or the
*/
/* ratio of hn(1)(kr2)/hn(2)(kr2) for pressure release condition
*/

    sphbes(n,(k*r2),&xsj,&xsy,&xsjp,&xsyp);
      a.r=xsjp;                               /*   a.r=xsj;  */
      a.i=xsyp;                               /*   a.i=xsy;  */
      b.r=xsjp;                               /*   b.r=xsj;  */
      b.i=-xsyp;                              /*   b.i=-xsy; */
    fprintf(f20,"%30s \n","The real and the imag. of hn'(1)/hn'(2) is:");
    fprintf(f20,"%f  %f \n",Cdiv(a,b).r,Cdiv(a,b).i);
/* Calculates The real and the imag. of hn2(kr1) */
    sphbes(n,(k*r1),&xsj,&xsy,&xsjp,&xsyp);
      hn2.r=xsj;
      hn2.i=-xsy;
    fprintf(f21,"%30s \n","The real and the imag. of hn2(r1) is:");
    fprintf(f21,"%f  %f \n",hn2.r,hn2.i);
/* Calculates The real and the imag.parts of the scattered pressure at the */
/* radius (r1) :Psc=-Pnm(costheta)*e^(imphi)*[hn'(1)(kr2)/hn'(2)(kr2)]*hn2(kr1)*/
      rp5=Cmul(RCmul(-Pnm,Cmul(Cdiv(a,b),Cexp(mphi))),hn2).r;
      rp6=Cmul(RCmul(-Pnm,Cmul(Cdiv(a,b),Cexp(mphi))),hn2).i;
```

```c
      fprintf(f22,"%f %f\n",rp5,rp6);
  }
        fclose(f4);
        fclose(f3);
        fclose(f5);
        fclose(f6);
        fclose(f7);
        fclose(f20);
        fclose(f21);
        fclose(f22);
        return 0;
}
#undef NRANSI


unsigned int factorial(unsigned int a)
{
      if((a==1)||(a==0))
      return 1;
  else
   {a*=factorial(a-1);
    return a;
    }
  }
***********************************************************************
```

APPENDIX B. FUNCTION INCPRE(X,Y,Z,K)

```
FUNCTION INCPRE(X,Y,Z,K)
*-------------------------------------------------------------------------
* PROGRAM BY ARTHUR LOBO DA COSTA RUIZ  12/23/93
* MODIFIED BY STEVEN R. BAKER 3/4/96
*-------------------------------------------------------------------------
* FUNCTION:
* COMPUTES THE INCIDENT SPHERICAL HARMONIC PRESSURE AT THE
*POINT (X,Y,Z),FOR THE WAVENUMBER K
* VARIABLES INPUT:
*          X,Y,Z: CARTESIAN COORDINATES OF THE POINT
*             K: WAVENUMBER
* VARIABLES OUTPUT:
*           RADIUS: R IN METERS
*           PHI IN DEGREES (HORIZONTAL ANGLE)
*           THETA IN RADIANS (AZIMUTAL ANGLE)
*           INCPRE : PRESSURE AT POINT IN PASCAL
*
* FORMULA USED:
*
*  INCPPRE=  H1(N)*P(M,N)*DCMPLX(DCOSD(M*PHI),DSIND(M*PHI))
*  THIS MAKES AN OUTGOING INCIDENT WAVE FOR  E^IWT  TIME
*  DEPENDENCE , AS FOR ATILA
*------------------------------------------------------------------
     DOUBLE PRECISION K,X,Y,Z,R,PHI,THETA,KR
     REAL*8 F1,PMN(-2:2,0:2),LOUT
     INTEGER N,M,NMAX
     COMPLEX*16 INCPRE,H1(0:2),H1OUT
* N AND M ARE ORDERS FOR HANKEL AND LEGENDRE FUNCTIONS
     N=0
     M=0
*  H1OUT AND LOUT ARE HANKEL AND LEGENDRE OUTPUTS
*  REF TO N AND M
     NMAX=2
* TRANSFORM CARTESIAN COORDINATES (X,Y,Z)
* INTO SPHERICAL COORDINATES
* R(RADIUS), PHI(AZIMUTAL ANGLE) AND THETA(POLAR ANGLE)
     R=DSQRT(X*X+Y*Y+Z*Z)
     PHI=DATAN2D(Y,X)
     IF((X.EQ.0).AND.(Y.EQ.0)) PHI=0.0D0
     THETA=DACOS(Z/R)
```

45

```fortran
      KR=K*R
* NMAX IS THE MAXIMUM NUMBER OF HARMONICS
      CALL HANKEL1(KR,NMAX,H1)
* SUBROUTINE HANKEL1 RETURNS SPHERICAL HANKEL
* FUNCTIONS OF THE FIRST KIND JN + I YN
      CALL LEGNDR(THETA,NMAX,PMN)
      LOUT=F1(N,M)*PMN(M,N)
* SUBROUTINE LEGNDR RETURNS ASSOCIATE LEGENDRE FUNTION
      H1OUT=H1(N)
      INCPRE=H1OUT*LOUT*DCMPLX(DCOSD(M*PHI),DSIND(M*PHI))
      IF ((R.LE.0.501).AND.(R.GT.0.499)) THEN
*   PRINT *,"X,Y,Z =",X,Y,Z
*   PRINT *,PHI,THETA
*   PRINT *,"K,R,KR =",K,R,KR
*   PRINT *,"REAL HANKEL1 =",H1OUT
*   PRINT *,"LEGENDRE =",LOUT
*    PRINT *,INCPRE
*    PRINT *,"***************"
      ELSE
      CONTINUE
      ENDIF
      RETURN
      END
C *************************************************************
      SUBROUTINE HANKEL1(X,NMAX,H1)
      IMPLICIT REAL*8 (A-H,O-Z)
      COMPLEX*16 H1(0:NMAX)

C  GIVEN THE VARIABLE X, AND THE MAXIMUM ORDER NMAX,
C  THIS ROUTINE GENERATES THE SPHERICAL HANKEL FUNCTION OF
THE
C  FIRST KIND H1N FOR ALL N FROM 0 TO NMAX (INCLUSIVE)
C  INPUT:
C    X = DOUBLE PREC. VARIABLE (RADIUS)
C    NMAX = INTEGER MAXIMUM ORDER OF BESSEL FUNCTIONS
DESIRED
C  OUTPUT:
C    H1(N) = ARRAY OF SPHERICAL HANKEL FUNCTIONS H1N(X), WHERE
C    H1N = JN + I YN
C    THIS ROUTINE IS BASED ON THE RECURSION FORMULA
C     FROM ABRAMOWITZ & STEGUN: 10.1.10 & 10.1.15, PP.438-9
C    THE F'S ARE THE COEFFICIENTS OF ORDER N & -(N+1),
C    THE FO'S ARE OLD F'S, FOR RECURSION
      IF ( X .LE. 0.0D0 ) THEN
```

```
      H1(0) = DCMPLX(1.0D0,-1.0D35)
      DO 2 N = 1, NMAX
         H1(N) = CMPLX(0.0D0,-1.0D35)
   2  CONTINUE
      RETURN
      END IF
      SX = DSIN(X)
      CX = DCOS(X)
      XINV = 1.0D0/X
      M1N = -1.0D0
      FN = XINV
      FMN = 0.0D0
      FNO = FMN
      FMNO = FN
      DO 4 N = 0, NMAX
      H1(N) = CMPLX( FN*SX + M1N*FMN*CX, -FN*CX + M1N*FMN*SX )
      T1 = (2*N+1)*XINV
      T2 = T1*FN - FNO
      FNO = FN
      FN = T2
      T2 = -T1*FMN - FMNO
      FMNO = FMN
      FMN = T2
      M1N = -M1N
   4  CONTINUE
      RETURN
      END
C ******************************************************************
      SUBROUTINE LEGNDR(THETA,NMAX,PMN)
      IMPLICIT REAL*8 (A-H,O-Z)
      REAL*8  F1,PMN(-NMAX:NMAX,0:NMAX)

C GIVEN THE VARIABLE THETA, AND THE MAXIMUM ORDER NMAX,
C  THIS ROUTINE GENERATES THE ASSOC. LEGENDRE FUNCTIONS PMN
C  OF THE ARGUMENT COS(THETA)  (THETA MUST BE BETWEEN 0 & PI)
C  FOR ALL N FROM 0 TO NMAX (INCLUSIVE)
C  AND FOR ALL M FROM -N TO N (SOME OTHERS SET TO ZERO)
C INPUT:
C   THETA = VARIABLE (POLAR ANGLE), MUST BE BETWEEN 0 & PI
(INCL.)
C   NMAX = INTEGER MAXIMUM ORDER OF LEGENDRE FUNCTIONS
C   DESIRED
C OUTPUT:
C   PMN = DOUBLE PREC. ARRAY, CONTAINS ASSOC. LEGENDRE FNS
```

```fortran
C  THIS ROUTINE IS BASED ON THE RECURSION FORMULAE
C     FROM ABRAMOWITZ & STEGUN
      X = DCOS(THETA)
      SINTHT = DSIN(THETA)
      IF ( SINTHT .GT. 0. ) THEN
        SININV = 1.0D0/SINTHT
      ELSE
        SININV = 0.0D0
      END IF
C  SET VALUES FOR N = 0, 1  (NMAX MUST BE AT LEAST 1)
      PMN(0,0) = 1.0D0
      PMN(1,0) = 0.0D0
      PMN(-1,0) = 0.0D0
      PMN(0,1) = X
      PMN(1,1) = -SINTHT
      PMN(-1,1) = SINTHT*0.5D0
C  IN LOOP, TNP1 = 2*N+1, TNP2FC = (2*N+2)!, M1N = (-1)**(N+1)
      TNP1 = 1.0D0
      TNP2FC = 2.0D0
      M1N = -1.0D0
      DO 4 N = 1, NMAX-1
        TNP1 = TNP1 + 2.0D0
        TNP2FC = TNP2FC * TNP1 * (TNP1+1)
        M1N = -M1N
        DO 3 M = -N, N
          PMN(M,N+1) = (TNP1*X*PMN(M,N) - (N+M)*PMN(M,N-1))/(N-M+1)
   3    CONTINUE
        PMN(N+1,N) = 0.0D0
        PMN(-N-1,N) = 0.0D0
        PMN(N+1,N+1) = (X*PMN(N,N+1) - TNP1*PMN(N,N)) * SININV
        PMN(-N-1,N+1) = M1N*PMN(N+1,N+1)/TNP2FC
   4  CONTINUE
      RETURN
      END
******************************
      FUNCTION F1(NN,MM)
      IMPLICIT REAL*8 (A-H,O-Z)
      REAL*8 FACT1,FACT2,PI
      PI=4.0D0*DATAN(1.0D0)
      FACT1=1.0D0
      DO 10 I=1,NN+MM
  10  FACT1=FACT1*I
      FACT2=1.0D0
      DO 20 I=1,NN-MM
```

```
20  FACT2=FACT2*I
    F1= DSQRT((2*NN+1)*FACT2/4.0D0/PI/FACT1)
    RETURN
    END
```

LIST OF REFERENCES

1.   Scandrett, C. L. and Canright, D. R., "Acoustic Interactions in Arrays of Spherical Elastic Shells", NPS Technical Report NPS-53-90-009, June 1990.

2.   Ruiz, A. L. C., "Calculation of the Transition Matrix for the Scattering of Acoustic Waves from a Thin Elastic Spherical Shell Using the ATILA F.E.C., Master's Thesis, NPS, Monterey, CA, 1994.

3.   Institut Superieur d'Electronique du Nord (ISEN), ATILA Finite Element Code for Piezoelectric and Magnetostrictive Transducer Modeling Version 5.03, User's Manual, September 1993.

4.   Davies, A. J., *The Finite Element Method: A First Approach*, Clarendon Press, Oxford, 1980.

5.   Zienkiewicz, O. C. and Taylor, R. L. *The Finite Element Method*, McGraw-Hill Book Company, Kerkshire, 1989.

6.   Fenner, Roger T., *Finite Element Methods for Engineers*, The MacMillan Press LTD, London, 1975.

7.   Schwartz, H. R., *Finite Element Methods*, Academic Press, London, 1988.

8.   Zienkiewicz, O. C. and Newton, R. F., "Coupled Vibrations of a Structure Submerged in a Compressible Fluid," Proceedings of the International Techniques, Stuttgart, 1969.

9.   Kinsler, L. E., Frey, A. R., Coppens, A. B. and Sanders, J. V., *Fundamentals of Acoustics*, John Wiley & Sons, 1982.

10.   Ziomek, L. J., *Fundamentals of Acoustic Field Theory and Space Time Signal Processing*, CRC Press, Inc., 1995.

11.   Press, W. H., Tenkolsky, S. A., Vetterling, W. T., and Flannery, B. P., *Numerical Recipes in C*, Second Edition, Cambridge University Press, 1992.

INITIAL DISTRIBUTION LIST